

# A coherent geostatistical approach for combining choropleth map and field data in the spatial interpolation of soil properties

P. GOOVAERTS

BioMedware, Inc., Ann Arbor, MI 48104, USA

## Summary

Information available for mapping continuous soil attributes often includes point field data and choropleth maps such as soil or geology maps that model the spatial distribution of soil attributes as the juxtaposition of polygons (areas) with constant values. This paper presents two approaches to incorporate both point and areal data in the spatial interpolation of continuous soil attributes. In the first instance, area-to-point kriging is used to map the variability within soil units while ensuring the coherence of the prediction so that the average of disaggregated estimates is equal to the original areal datum. The resulting estimates are then used as local means in residual kriging. The second approach proceeds in one step and capitalizes on (i) a general formulation of kriging that allows the combination of both point and areal data through the use of area-to-area, area-to-point and point-to-point covariances in the kriging system, (ii) the availability of Geographical Information Systems (GIS) to discretize polygons of irregular shape and size and (iii) knowledge of the point-support variogram model that can be inferred directly from point measurements, thereby eliminating the need for deconvolution procedures. The two approaches are illustrated using the geological map and heavy metal concentrations recorded in the topsoil of the Swiss Jura. Sensitivity analysis indicates that the new procedures improve prediction over ordinary kriging and traditional residual kriging based on the assumption that the local mean is constant within each mapping unit.

## Introduction

Prediction of soil properties at unsampled locations can be accomplished by using two main models: soil classification linked to a soil map and spatial interpolation (Voltz & Webster, 1990). Soil maps, as all choropleth maps, model the spatial distribution of soil attributes as the juxtaposition of polygons with constant values. This representation is built on the assumption that each mapping unit is relatively homogeneous and that sharp differences occur at their boundaries (Webster & Beckett, 1968). The advent of geostatistics, combined with more affordable sampling and measurement procedures, has led to the wide adoption of continuous representations (isopleth maps) for soil properties where all variation is gradual (Burgess & Webster, 1980). Semivariogram inference and kriging are, however, based on the assumption of stationarity, which might not be appropriate for heterogeneous areas where both gradual and abrupt changes are likely to take place. In addition, soil maps contain precious expert knowledge that should not be ignored, in particular in sparsely sampled areas.

Recognizing the value of soil map information, geostatisticians have proposed several approaches to incorporate both mapping units and point measurements in the prediction of soil properties. In the first case, the soil map is used to delineate homogeneous regions or strata that will undergo a separate geostatistical analysis (McBratney *et al.*, 1991). Unsampled locations are then predicted by using only the observations belonging to the same stratum and a semivariogram that is either stratum-specific (Stein *et al.*, 1988) or is a combination of all within-stratum semivariograms (Voltz & Webster, 1990; Van Meirvenne *et al.*, 1994). Such kriging within strata, however, produces maps with sharp discontinuities at the strata boundaries and its prediction performance depends on the nature of soil map delineation (Brus *et al.*, 1996; Boucneau *et al.*, 1998). In addition, the interpolation accounts only for the boundaries of the mapping unit and ignores the representative value of the soil attributes typically available for each unit.

These limitations are overcome by a second approach where soil map information is used to estimate the local mean of the random function (Goovaerts & Journel, 1995; Hengl *et al.*, 2004; Liu *et al.*, 2006). Variography and kriging are thus conducted on the stationary residuals (differences between point measurements and mapping unit means) that can be combined across soil boundaries.

Correspondence: P. Goovaerts. E-mail: goovaerts@biomedware.com

Received 10 September 2009; revised version accepted 28 February 2011

This form of residual kriging still relies on the assumption that the local mean is constant across each mapping unit. Another way to incorporate soil map information into the kriging of field measurements was proposed by Heuvelink & Bierkens (1992), who computed a weighted average of soil map predictions and predictions obtained from kriging the observations. Weights can be selected to reflect the accuracy of the two sets of values, with the contribution of each source inversely proportional to its error variance. Although a validation study demonstrated the benefit of this approach over the separate use of the soil map or the kriged map, the weighted estimator is heuristic because soil map and kriging predictors assume different statistical models.

This paper presents a coherent geostatistical approach to accommodate both areal and point data in the spatial interpolation of continuous soil properties. Two variants of the same geostatistical model are introduced. In the first case, 'area-to-point' (ATP) kriging (Kyriakidis, 2004) is used to map the variability within geographical units while ensuring the coherence of the prediction so that the sum or average of disaggregated estimates is equal to the original areal datum. The resulting estimates are then used as local means in residual kriging. The second approach proceeds in one step and capitalizes on, first, a general formulation of kriging that allows the combination of both point and areal data through the use of area-to-area, area-to-point and point-to-point covariances in the kriging system. Second, it uses the availability of GIS to discretize polygons of irregular shape and size. Third, the knowledge of the point-support variogram model can be inferred directly from point measurements, thereby eliminating the need for a deconvolution procedure (Goovaerts, 2008). A similar approach was recently implemented within a stochastic simulation framework by Liu & Journel (2009). Their algorithms (direct sequential simulation and error simulation) are capable of handling different block geometries and different layouts of block data, including irregular-shaped and overlapping blocks.

The procedure is illustrated by using the geological map and heavy metal concentrations recorded in the topsoil of the Swiss Jura (Goovaerts, 1997). The performance of the proposed approaches, relative to ordinary kriging or a traditional residual kriging with a choropleth trend model, is assessed by using jackknifing. Performance criteria include the magnitude of prediction errors, the accuracy of the model of uncertainty and the ability to discriminate between hazardous and safe areas.

## Materials and methods

### The Jura dataset

The combination of point field data and areal map data in spatial interpolation is illustrated by using a case-study related to heavy metal contamination of an area of the Swiss Jura. In the spring of 1992, the Swiss Federal Institute of Technology surveyed the topsoil of a 14.5-km<sup>2</sup> region near la Chaux-de-Fonds and measured the concentrations of seven trace metals at 359 locations (Atteia *et al.*, 1994; Figure 1a). Webster *et al.* (1994) investigated the effect of geological formation and land

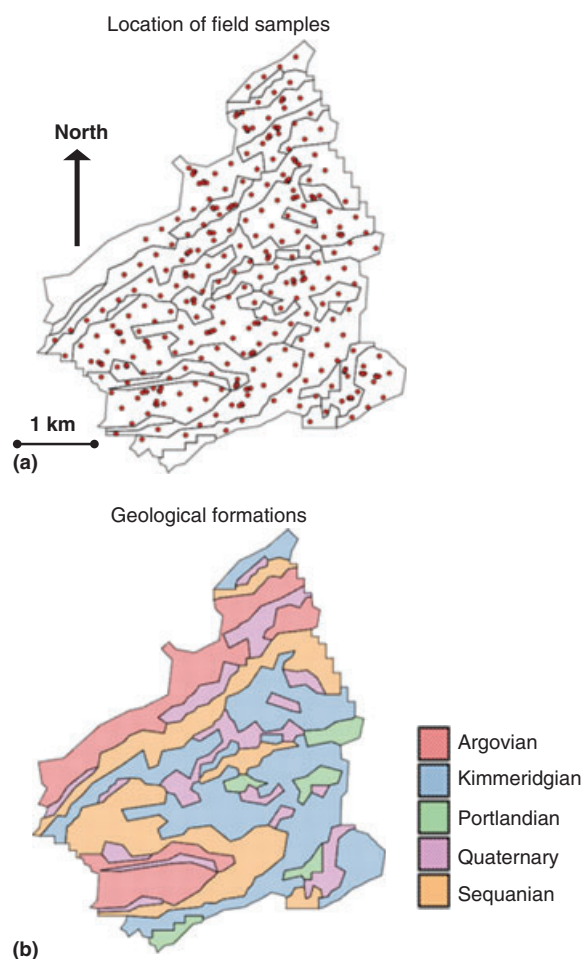


**Figure 1** Information available for mapping topsoil heavy metal concentration. (a) Field measurements collected at 359 point locations. (b) Choropleth map of the main geological formations.

use on topsoil metal concentrations and found that cadmium, cobalt and nickel concentrations were related to geology; in particular, much smaller concentrations were recorded on the Argovian formation. The geological map displayed in Figure 1(b) thus acts as our source of areal information. This map includes 35 polygons that belong to one of the five geological formations. The mean metal concentration within each formation was computed as the weighted average of all samples collected on that formation (Figure 3c). The weighting is the area of influence of each sample (Thiessen polygon) in order to account for data clustering. In situations where a soil map is available, areal data would simply be identified with concentrations recorded on representative profiles for each mapping unit.

### Residual kriging

Consider the problem of estimating the value of a soil property  $z$  at any location  $\mathbf{u}$  within a study area  $A$ . The information available consists of a set of field data collected at  $n$  discrete locations  $\mathbf{u}_\alpha$  ( $z(\mathbf{u}_\alpha)$ ;  $\alpha = 1, \dots, n$ ), supplemented by a set of  $B$  areal data

( $z(v_\beta)$ ;  $\beta = 1, \dots, B$ ) recorded for mapping units  $v_\beta$  of various sizes and shapes. The first class of interpolation methods uses the areal data to gather information about the local mean of the random variable  $Z$  at both sampled and unsampled locations. The predicted value at location  $\mathbf{u}$ ,  $z^*(\mathbf{u})$ , is thus computed as the following linear combination of residuals  $r(\mathbf{u}_\alpha)$  plus the local mean  $m^*(\mathbf{u})$ :

$$\begin{aligned} z_{RK}^*(\mathbf{u}) &= m^*(\mathbf{u}) + \sum_{\alpha=1}^{n(\mathbf{u})} \lambda_\alpha [z(\mathbf{u}_\alpha) - m^*(\mathbf{u}_\alpha)] \\ &= m^*(\mathbf{u}) + \sum_{\alpha=1}^{n(\mathbf{u})} \lambda_\alpha r(\mathbf{u}_\alpha). \end{aligned} \quad (1)$$

The weights  $\lambda_\alpha$  assigned to the  $n(\mathbf{u})$  neighbouring observations are solutions of the following system of  $n(\mathbf{u})$  linear equations, known as a simple kriging system:

$$\sum_{\beta=1}^{n(\mathbf{u})} \lambda_\beta C_R(\mathbf{u}_\alpha - \mathbf{u}_\beta) = C_R(\mathbf{u}_\alpha - \mathbf{u}) \quad \alpha = 1, \dots, n(\mathbf{u}), \quad (2)$$

where  $C_R(\mathbf{h})$  is the covariance of the residual random function  $R(\mathbf{u}) = Z(\mathbf{u}) - m^*(\mathbf{u})$ . Independence between the local mean and the residual random function is assumed, and the prediction variance is therefore computed as the sum of the estimation variance for the local mean and the residual kriging variance:

$$\sigma_{RK}^2(\mathbf{u}) = \sigma_m^2(\mathbf{u}) + C_R(0) - \sum_{\alpha=1}^{n(\mathbf{u})} \lambda_\alpha C_R(\mathbf{u}_\alpha - \mathbf{u}). \quad (3)$$

The most straightforward approach is to estimate the local mean  $m^*(\mathbf{u})$  by the areal datum recorded for the mapping unit that includes  $\mathbf{u}$ :  $m^*(\mathbf{u}) = z(v_\beta)$  if  $\mathbf{u} \in v_\beta$ . Similarly,  $\sigma_m^2(\mathbf{u})$  is estimated by the prediction variance for that unit's local mean, which, for the Jura dataset, is the area-weighted variance divided by the number of observations on the geological formation. The underlying assumption is that the local mean of the soil property is constant within each unit and suddenly changes at the boundary between two mapping units, which is not realistic for most continuous variables (Burrough, 1986) and ignores the uncertainty attached to the delineation of these units.

An alternative approach to the use of choropleth maps of local means is to create continuous or isopleth maps, which requires a model for the intra-unit variation of  $z$  within any unit  $v_\beta$ . Such modelling can be viewed as a disaggregation of the corresponding areal datum  $z(v_\beta)$  into a set of  $P_\beta$  point estimates  $z^*(\mathbf{u}_s)$ , where  $P_\beta$  is the number of discretizing points within unit  $v_\beta$ . These discretizing points would typically be the nodes of a regular grid for mapping purposes. A desirable property of such disaggregation would be its coherency so that the aggregation of the  $P_\beta$  point estimates within any given entity  $v_\beta$  must return the areal datum

$$z(v_\beta) = \frac{1}{P_\beta} \sum_{s=1}^{P_\beta} z^*(\mathbf{u}_s). \quad (4)$$

In the presence of spatial auto-correlation, it would be useful for the point estimates to vary smoothly within each mapping unit and across boundaries between units.

Area-to-point (ATP) kriging, which is simply the counterpart of block kriging in that point estimates are now obtained from areal (block) measurements, fulfills these conditions. The ATP kriging estimate for any given point  $\mathbf{u}_s$  is expressed as follows:

$$z_{ATP}^*(\mathbf{u}_s) = \sum_{k=1}^K \lambda_k(\mathbf{u}_s) z(v_k), \quad (5)$$

where  $K$  is typically smaller than the total number of areal data  $B$  and corresponds, for example, to the blocks adjacent to the block  $v_\beta$  where the point estimation is conducted. The constraint in Equation (4) is satisfied if the same  $K$  areal data are used for prediction at each location within the set of  $P_\beta$  discretizing point  $\mathbf{u}_s$ . The kriging weights are the solution of the following ordinary kriging system:

$$\begin{aligned} \sum_{k'=1}^K \lambda_{k'}(\mathbf{u}_s) \overline{C}(v_k, v_{k'}) + \mu(\mathbf{u}_s) &= \overline{C}(v_k, \mathbf{u}_s) \quad k = 1, \dots, K \\ \sum_{k'=1}^K \lambda_{k'}(\mathbf{u}_s) &= 1, \end{aligned} \quad (6)$$

where  $\mu(\mathbf{u}_s)$  is the Lagrange multiplier. As in traditional block kriging, the block-to-point covariances  $\overline{C}(v_k, \mathbf{u}_s)$  are approximated by the average of the point support covariance  $C(\mathbf{h})$  computed between the location  $\mathbf{u}_s$  and a set of  $P_k$  points discretizing the block  $v_k$  (Figure 2a). A similar procedure is used for the block-to-block covariances  $\overline{C}(v_k, v_{k'}) = \text{Cov}\{Z(v_k), Z(v_{k'})\}$  and involves averaging  $C(\mathbf{h})$  computed between any two points discretizing the blocks  $v_k$  and  $v_{k'}$  (Figure 2b). When the size of mapping units differs by several orders of magnitude, as for the Jura dataset, it is not computationally efficient to use the same discretizing level for each unit. One solution is to use flexible discretizing grids that ensure a constant number of discretizing points within each unit. Figure 2(c) gives an example where 50 points are used for each of the 35 polygons. The trade-off cost for shorter computational times is that the constraint in Equation (4) is not exactly met because interpolation grid nodes and discretizing points are no longer the same.

While the local mean  $m^*(\mathbf{u})$  is identified with the ATP kriging estimate, the variance  $\sigma_m^2(\mathbf{u})$  is estimated by the ATP kriging variance computed as

$$\sigma_{ATP}^2(\mathbf{u}_s) = C(0) - \sum_{k=1}^K \lambda_k(\mathbf{u}_s) \overline{C}(v_k, \mathbf{u}_s) - \mu(\mathbf{u}_s). \quad (7)$$

Kyriakidis (2004) demonstrated that the choropleth map approach is in fact a particular case of ATP kriging in that it corresponds to the solution of the kriging system in Equation (6) when the attribute values are spatially uncorrelated.

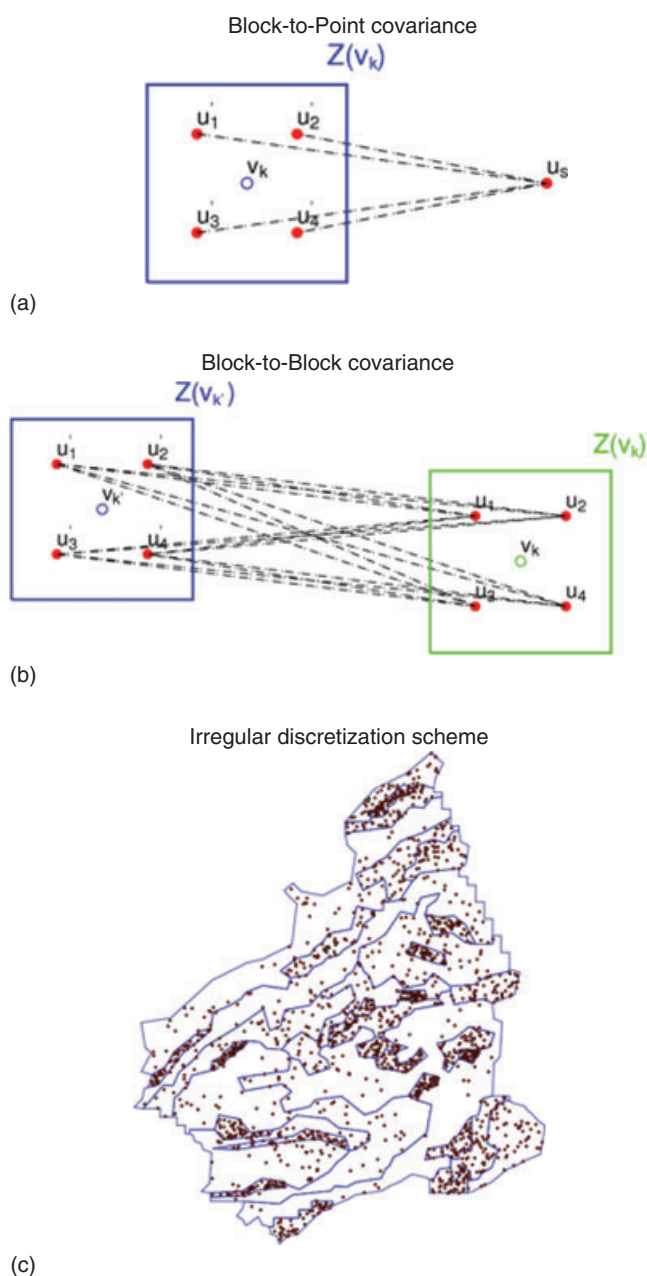


**Figure 2** Computation of covariance values in ATP and AAP kriging. The block-to-point covariance (a) and the block-to-block covariance (b) are approximated by the average of point-to-point covariances computed between points discretizing each block. (c) Example of discretization scheme adopted for blocks of irregular size and shape: 50 points randomly distributed within each mapping unit.

### Area-and-point kriging

Because residual kriging proceeds in two steps, the coherency of the ATP kriging estimates is lost when they are combined with residual estimates in Equation (1). However, there is no theoretical obstacle to the combination of both areal and point data in the same kriging expression. The so-called area-and-point

(AAP) kriging estimate is written as follows:

$$z_{AAP}^*(\mathbf{u}) = \sum_{\alpha=1}^{n(\mathbf{u})} \lambda_{\alpha}(\mathbf{u})z(\mathbf{u}_{\alpha}) + \sum_{k=n(\mathbf{u})+1}^{n(\mathbf{u})+K} \lambda_k(\mathbf{u})z(v_k). \quad (8)$$

The kriging weights are the solution of the following ordinary kriging system:

$$\sum_{j=1}^{n(\mathbf{u})+K} \lambda_j(\mathbf{u})\bar{C}(x_i, x_j) + \mu(\mathbf{u}) = \bar{C}(x_i, \mathbf{u}) \quad i = 1, \dots, n(\mathbf{u}) + K$$

$$\sum_{j=1}^{n(\mathbf{u})+K} \lambda_j(\mathbf{u}) = 1, \quad (9)$$

where  $x_i = \mathbf{u}_i$  if  $i \leq n(\mathbf{u})$ , and  $x_i = v_i$  otherwise. The quantity  $\bar{C}(x_i, x_j)$  represents a point-to-point, point-to-block or block-to-block covariance depending on the indices  $i$  and  $j$ . If the covariance function of the areal data is not derived by regularization of the covariance of the point data (for example where the experimental semivariogram of areal data is modelled directly), the kriging system in Equation (9) should be viewed as a co-kriging system and the conditions described in Pardo-Iguzquiza *et al.* (2010) should be imposed on the set of (cross)-covariance functions to ensure the positive semi-definiteness of the covariance matrix.

The coherency constraint in Equation (4) is satisfied if the same  $K$  areal data and  $n(\mathbf{u})$  point data are used for prediction at each  $P_{\beta}$  discretizing point  $\mathbf{u}_{\beta}$  within the unit  $v_{\beta}$ . This condition is fulfilled by conducting the search for closest areal and point neighbours on the basis of the distance to the centroid of the unit  $v_{\beta}$ . For small  $n(\mathbf{u})$  this search option can create discontinuities away from the unit's centroids, because the interpolation might not be based on the closest observations.

### Performance comparison study

The prediction performances of the different interpolation techniques with respect to sampling density were investigated using the following procedure.

1. Selection of a random subset of  $n$  field data with  $30 \leq n \leq 165$  (prediction set). For each of the 10 sampling intensities, 100 different random subsets were selected to account for sampling fluctuations.
2. For each random subset and sampling intensity:
  - (i) Prediction of the heavy metal concentration at the  $N = 369 - n$  remaining locations (validation set) using each of the four algorithms and a similar search strategy to that applied in Figure 3. Here a minimum separation distance of 250 m was imposed on neighbouring field data to avoid overly optimistic prediction accuracies for clustered observations and a coarser discretization geography (a 100-m instead of a 25-m grid) was used

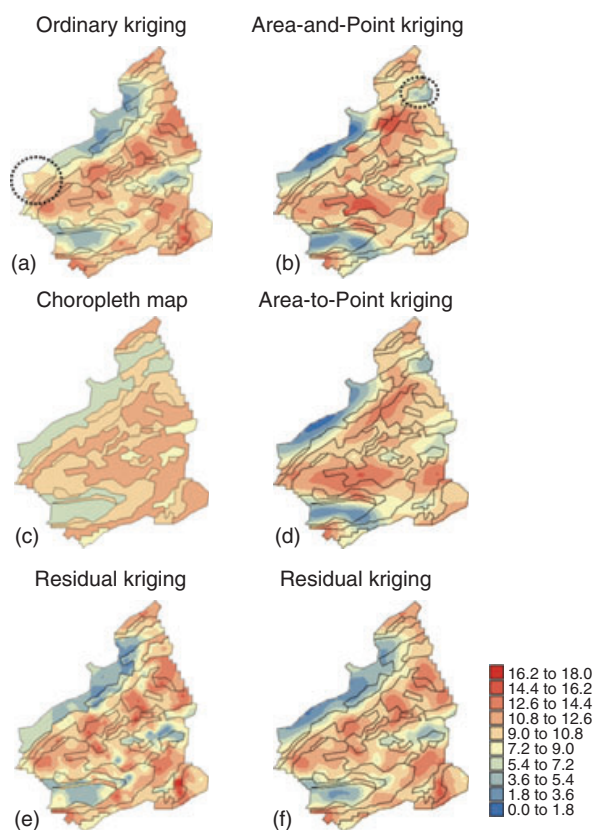


**Figure 3** Maps of cobalt concentration created by alternative interpolation techniques. (a) Ordinary kriging. (b) Kriging that combines both point and areal data. (e,f) Residual kriging uses two different types of trend model: (c) a choropleth trend model, and (d) a continuous trend estimated using area-to-point kriging. The legend (units =  $\text{mg kg}^{-1}$ ) applies to all maps.

to reduce the computational time required by each of the 1000 simulation runs. In each case, the experimental semivariogram was computed and modelled by using weighted least-square regression.

- (ii) Computation of the mean absolute error (MAE) of prediction as

$$MAE = \frac{1}{N} \sum_{\alpha=1}^N |z^*(\mathbf{u}_{\alpha}) - z(\mathbf{u}_{\alpha})|. \quad (10)$$

- (iii) Computation of the mean square standardized residual (MSSR) as

$$MSSR = \frac{1}{N} \sum_{\alpha=1}^N \left[ \frac{z^*(\mathbf{u}_{\alpha}) - z(\mathbf{u}_{\alpha})}{\sigma_K(\mathbf{u}_{\alpha})} \right]^2. \quad (11)$$

If the actual estimation error is equal, on average, to the error predicted by the model, the MSSR statistic should be approximately one (Wackernagel, 1998). To penalize equally the over- and under-estimation of the prediction errors by the kriging variance, the inverse of MSSR was considered if it exceeded one.

- (iv) Classification of each of the  $N$  test locations as hazardous or safe based on the exceedance of a threshold by the estimated concentration, and computation of the proportion of misclassified locations (sum of false positives and false negatives).

## Results and discussion

### Mapping cobalt concentration using point kriging

Figure 3 shows the maps of cobalt concentration estimated on a square grid of spacing 25 m and using alternative interpolation techniques. The reference approach is ordinary kriging (OK) that uses only the 369 field data (Figure 3a). At each grid node, the estimation was based on the 16 closest observations and the anisotropic model fitted to the directional semivariograms (Figure 4a). The variability increases more slowly in the NE–SW direction. This anisotropy reflects the impact of geological formation on the spatial distribution of cobalt concentrations, because NE–SW corresponds to the preferential orientation of geological layers (Figure 1b). The OK map depicts the regional trend in cobalt concentration, in particular the smaller values on the Argovian formation. Although the estimates represent field data at their locations, the average of kriging estimates within each mapping unit displays large fluctuations even among units of the same geological formation (Figure 5a). In addition, in sparsely sampled zones such as that delineated by a dashed circle in Figure 3(a), it should be the aim to incorporate information on the prevailing geological formation. In the present case, the occurrence of the Argovian formation suggests probable smaller concentrations than those recorded in close vicinity but on other formations.

### Mapping cobalt concentration using areal and point data

Figure 3(c) shows the set of areal data that was created by allocating the area-weighted averages of field concentrations to each of the five geological formations. In particular, note the much smaller average cobalt concentrations recorded on the Argovian formation. A possibly more realistic representation of the spatial trend in cobalt concentration is displayed in Figure 3(d). This isopleth map was obtained by using ATP (area-to-point) kriging and the same anisotropic semivariogram model as for ordinary kriging. The areal information consisted of units that are first and second order neighbours of the ‘kernel’ mapping unit  $v_{\beta}$  that includes the estimation grid node. The computation of area-to-area and area-to-point covariances was based on a discretization of each mapping unit using the interpolation grid nodes, which ensures that the ATP estimates honour the coherency constraint. In other words, averaging the values within each mapping unit of Figure 3(d) returns the choropleth map of Figure 3(c). The influence of the coherency constraint on the interpolation strongly depends on the geometry (size and shape) of the mapping units. For the Jura dataset several units, such as the Argovian formation in the north of the study region, are large and elongated, leading to a wide range of ATP cobalt concentration estimates; for

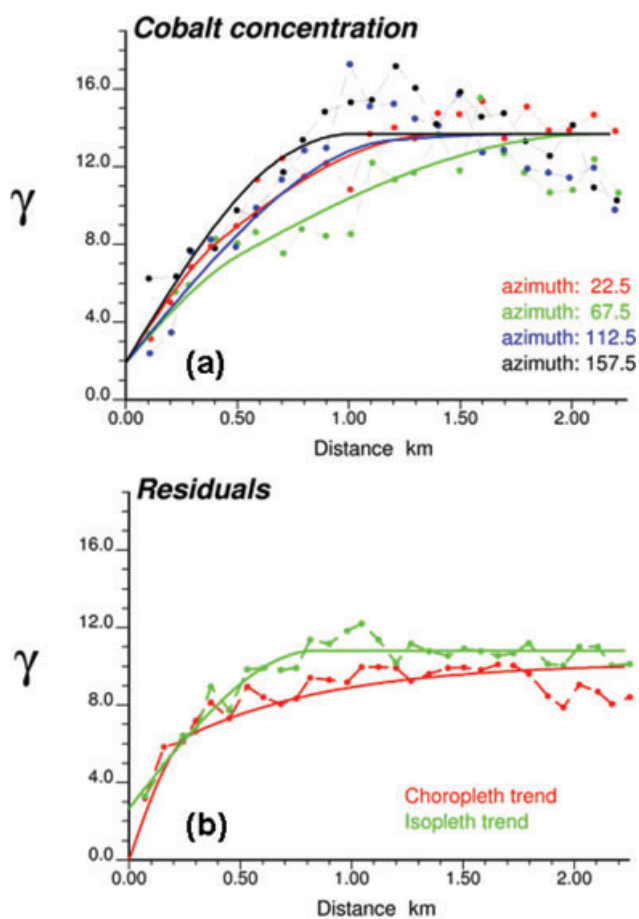


**Figure 4** Semivariogram models used for geostatistical interpolation. (a) Anisotropic model fitted to semivariograms of cobalt concentration. (b) Isotropic model fitted to semivariogram of residuals computed for choropleth and isopleth maps of trend estimates.

example, larger estimates in the north and smaller estimates in the south (Figure 3d). However, a small change to the boundary of the Quaternary formation would divide the Argovian formation into two mapping units and cause a substantial change to the predicted map, because the mean within both parts of the Argovian formation would be constrained to the formation average.

Both types of trend model were subtracted from the field cobalt concentrations and the semivariograms of the resulting residuals are displayed in Figure 4(b). As expected, the residual semivariograms have smaller values than the original semivariogram of Figure 4(a) because part of the total variance is captured by the trend models. In this example, the choropleth map accounts for a slightly larger part of the variance. Residuals were interpolated using simple kriging and the isotropic semivariogram models in Figure 4(b) and their combination with the trend models yielded the kriged maps in Figure 3(e,f). Differences between the two residual kriging maps and ordinary kriging are largest in sparsely sampled areas where the choice of a trend model becomes highly relevant (Goovaerts, 1997). In particular, incorporating the geological information leads to smaller estimates in the section of

Argovian formation where no sample was collected (dashed circle in Figure 3a). Because the residual semivariogram model fitted for the choropleth trend model has no nugget effect and a small range, the resulting map (Figure 3e) displays smaller features centred around sampled locations than the smoother map (Figure 3f) that is based on ATP kriging.

Scatter plots in Figure 5(c,d) indicate that residual kriging (RK) reduces somewhat the inconsistencies between choropleth map information and the average of concentration estimates within each mapping unit. However, there is no guarantee that the coherency constraint will be honoured once the kriged residuals have been added to the trend estimates. Such constraint can only be imposed through the joint incorporation of point field data and areal map data by AAP kriging. The areal information consisted of units that are first- and second-order neighbours of the kernel mapping unit  $v_\beta$ . The number of field data was the same as for ordinary kriging but they were selected according to their proximity to the centroid of unit  $v_\beta$  to ensure that the same observations were used for all nodes within  $v_\beta$ , which is required for the AAP estimates to honour the coherency constraint (Figure 5b). In other words, averaging the values within each mapping unit of Figure 3(b) results in the choropleth map of Figure 3(c).

The map of AAP kriging estimates shares similar features with the ATP trend map (Figure 3d); for example, small concentrations are predicted for the smallest Argovian unit in the northeast of the study area (dashed circle in Figure 3b). Those features were lost, along with the coherency constraint, when combining the trend estimates with the residual estimates to create the map of Figure 3(f). To understand better the relative contributions of point and areal data, three types of kriging weights were computed and mapped in Figure 6. The sum of weights of point data is the largest and generally positive around clusters of field observations (Figure 6a), while the kernel areal datum receives a larger weight in sparsely sampled areas, such as along the edges of the study area (Figure 6b). Because of the screening effect, the other areal data (adjacent mapping units) receive much smaller weights although their contribution increases at the edges of the mapping unit. This is particularly the case for larger kernel units when the distance to the centroid tends to be the largest (Figure 6c). This increase ensures smooth transitions across unit boundaries, as illustrated in Figure 3(d). Under the coherency and unbiased kriging constraints, within each mapping unit the weights of kernel areal data average one while the mean weights for point data and adjacent areal data are zero (Goovaerts, 2008). These constraints explain why the sum of the weights for point data is negative over half the grid nodes.

#### Mapping the prediction variance

Figure 7 shows the maps of prediction variance associated with the cobalt concentration maps of Figure 4. The variance for residual kriging (Figure 7e,f) was computed as the sum of the simple kriging variance for residuals interpolation and the variance associated with the trend model (Figure 7c,d). Because the same

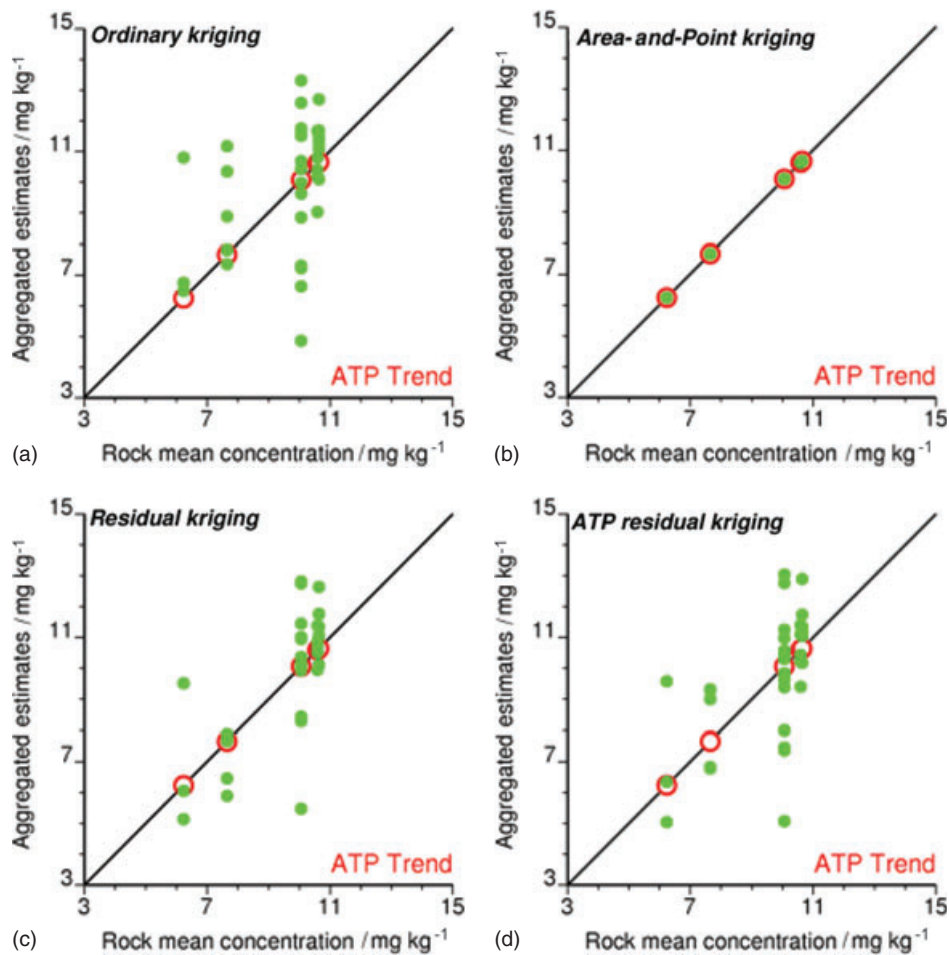


**Figure 5** Scatterplots of areal cobalt concentrations versus averages of kriging estimates within each mapping unit. Only area-and-point kriging ensures the reproduction of areal data (b), while other interpolation techniques (a, c, d) do not honour the coherency constraint.

legend is used for all six maps and the variances associated with the choropleth trend model are much smaller than the other variances based on kriging, the map in Figure 7(c) appears to be uniform. The prediction variance maps for OK and RK using the choropleth trend model (Figure 7a,e) look to be similar, with smaller variances in the vicinity of field data and larger variances in extrapolation situations (along the edges of the study area).

When only areal data are used (ATP kriging), the kriging variance depends mainly on the proximity to the centre of the mapping units and is thus less in smaller and more compact units (Figure 7c). Combining the ATP kriging variance with the RK variance yields much larger variances than the other kriging approaches (Figure 7f). This result is partially caused by the negative correlation between residuals and local mean ( $-0.34$ ) for cobalt, in violation of the assumption of independence used to compute the prediction variance according to Equation (3). The map of AAP kriging variances (Figure 7b) displays features of both OK and ATP maps: smaller variances in smaller mapping units and in the vicinity of field samples.

#### Performance comparison study

Figures 3–7 support an empirical comparison of results obtained using ordinary kriging versus residual kriging and area-and-point kriging. However, because the ‘true’ cobalt concentration is unknown, it cannot be concluded that one approach outperforms the other. The prediction performances of the different interpolation techniques with respect to sampling density were investigated using the procedure described earlier. This procedure was applied to cadmium concentrations because this metal is the most impacted by the geology among the seven variables of the Jura dataset (Atteia *et al.*, 1994) and the tolerable maximum of  $0.8 \text{ mg kg}^{-1}$  is exceeded in 64.9% of the data (Goovaerts, 1997).

Figure 8 indicates that over the 100 random subsets the simultaneous incorporation of areal and point data using AAP kriging is the most likely to give the best results for all three performance criteria: it has the smallest mean absolute error of prediction and misclassification rate on average while the average mean square standardized residual (MSSR) is the closest to 1. Residual kriging using the ATP kriging trend model is the second best, except for the MSSR statistic: the sum of

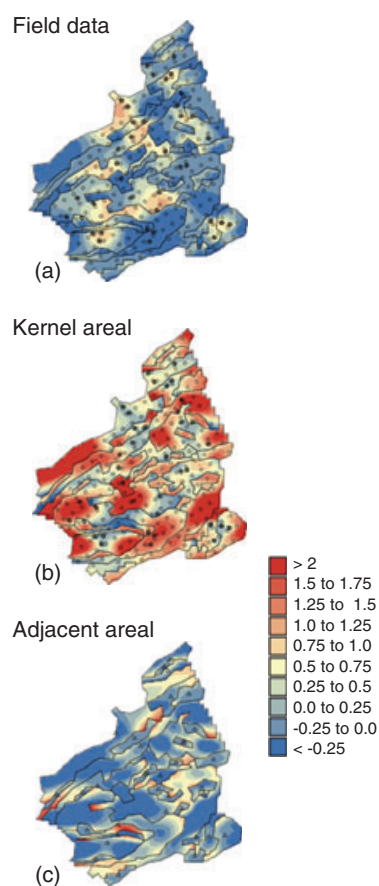


**Figure 6** Maps of area-and-point (AAP) kriging weights assigned to different types of data in the mapping of cobalt concentration in Figure 3(b). (a) Field data (sum for 16 observations). (b) Kernel areal datum. (c) Neighbouring areal data (second-order adjacency). Open circles denote the location of field data while open triangles correspond to centroids of mapping units.

the ATP kriging variance and the RK variance clearly overestimates the magnitude of prediction errors, leading to a very small MSSR. This latest result confirms the interpretation of Figure 7(f), although the correlation between residual and local mean is negligible for cadmium. The choropleth map yields the worst estimates for all sample sizes and statistics; in particular, the MSSR statistic is so large (over 7.5) that it is not plotted in Figure 8(c). For ordinary kriging, the absolute prediction error and misclassification rates decrease as the sample size increases.

## Conclusions

A common issue in spatial interpolation of soil properties is the incorporation of data measured at various scales and over different spatial supports. This situation is frequently encountered when we wish to combine measurements at discrete locations in the field with a choropleth classification linked to a soil map. Whereas the first analytical developments of kriging clearly demonstrated its ability to accommodate different measurement and prediction

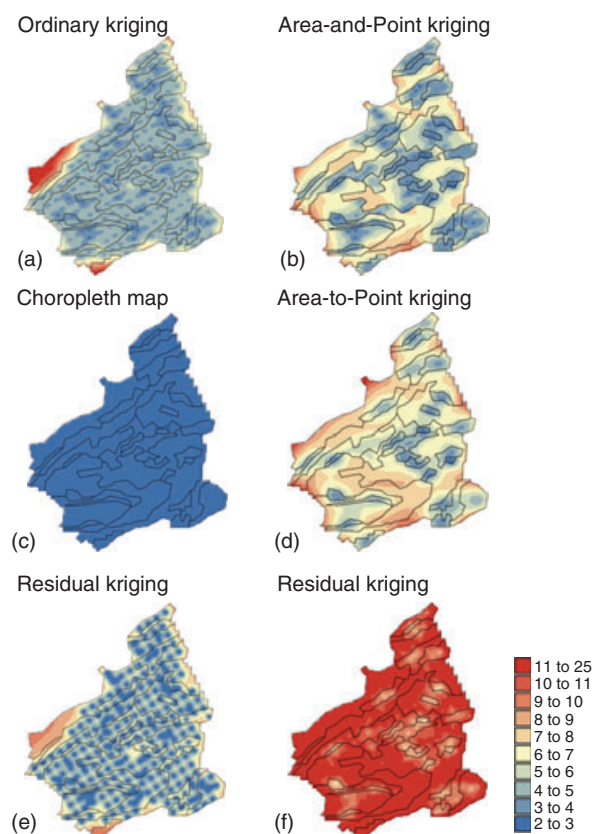


**Figure 7** Maps of prediction variance associated with the maps of Figure 3. (c,d) Trend models. (a–f) Kriging estimates.

supports, geostatistical analysis of a mixture of point data and irregular blocks has rarely been implemented, mainly because of its lack of application in mining. Because of the joint advances of GIS software and computational resources, it is possible to move beyond the simplified kriging of point data or regular blocks adopted in the early days of geostatistics, and generalize kriging to the complex geographies encountered in soil classification.

Geostatistics provides a framework to model the spatial correlation among soil properties measured over irregular geographical supports, allowing the mapping of the distribution of attribute values within each soil unit while fulfilling the coherency constraint. Such isopleth maps provide a more realistic trend model than the choropleth map of local means typically used in residual or regression kriging. Unlike the heuristic weighted average described by Heuvelink & Bierkens (1992), the proposed approach takes into account both the spatial support and pattern of spatial autocorrelation in the computation of weights assigned to each piece of information. Whereas stratified kriging typically causes sharp discontinuities in the interpolated maps, area-and-point kriging avoids sharp changes in estimated values at the borders between units by allowing the incorporation of field data belonging to adjacent mapping units. Sensitivity analysis demonstrated the overall better prediction performance of the proposed approaches over ordinary kriging and residual kriging with the choropleth map

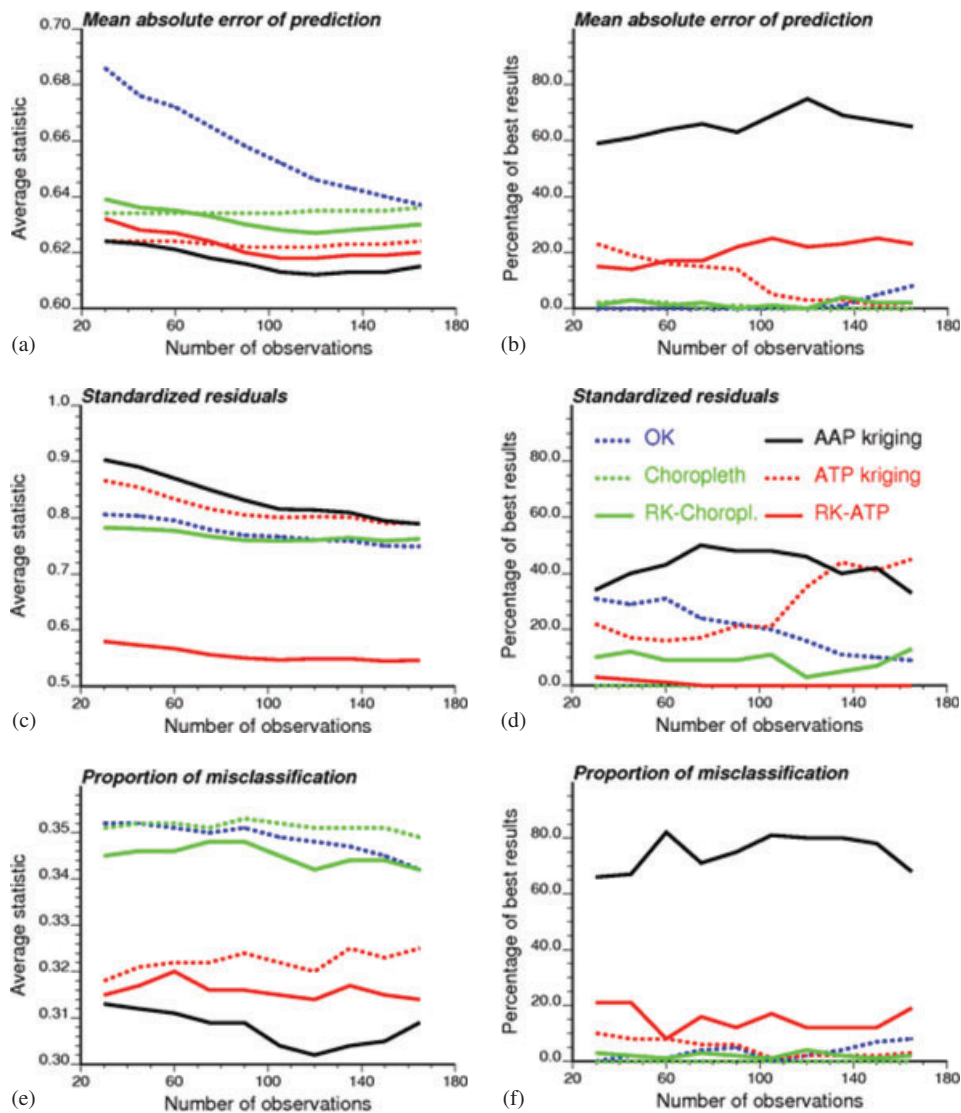


**Figure 8** Impact of the sample size on the average value of the performance statistic and the percentage of simulations for which an interpolation technique outperforms the other five. Cross-validation statistics include: (a,b) the mean absolute error of prediction, (c,d) the mean square standardized residual, (e,f) the proportion of misclassified observations with respect to the physical threshold of  $0.8 \text{ mg kg}^{-1}$ .

trend model, in particular when sampling is sparse. Similar results were recently obtained for the Northern Ireland dataset described by Rawlins *et al.* (2009). Cross-validation (Kerry *et al.*, 2010) demonstrated the benefit of using the ATP trend model compared with the choropleth map in the regional mapping of soil organic carbon by residual kriging.

### Acknowledgements

This research was funded by grants R43-CA135814-01 and R44-CA132347-02 from the National Cancer Institute. The views stated in this publication are those of the author and do not necessarily represent the official views of the NCI. The author thanks the Guest Editor and two anonymous reviewers for their very pertinent comments.

### References

- Atteia, O., Dubois, J.-P. & Webster, R. 1994. Geostatistical analysis of soil contamination in the Swiss Jura. *Environmental Pollution*, **86**, 315–327.
- Boucaeu, G., Van Meirvenne, M., Thas, O. & Hofman, G. 1998. Integrating properties of soil map delineations into ordinary kriging. *European Journal of Soil Science*, **49**, 213–229.
- Brus, D.J., De Gruijter, J.J., Marsman, B.A., Visschers, R., Bregt, A.K., Breeuwsma, A. *et al.* 1996. The performance of spatial interpolation methods and choropleth maps to estimate properties at points: a soil survey case study. *Environmetrics*, **7**, 1–16.
- Burgess, T.M. & Webster, R. 1980. Optimal interpolation and isarithmic mapping of soil properties. I. The semi-variogram and punctual kriging. *Journal of Soil Science*, **31**, 315–331.

- Burrough, P.A. 1986. *Principles of Geographical Information Systems for Land Resources Assessment*. Clarendon Press, Oxford.
- Goovaerts, P. 1997. *Geostatistics for Natural Resources Evaluation*. Oxford University Press, New York.
- Goovaerts, P. 2008. Kriging and semivariogram deconvolution in presence of irregular geographical units. *Mathematical Geosciences*, **40**, 101–128.
- Goovaerts, P. & Journel, A.G. 1995. Integrating soil map information in modeling the spatial variation of continuous soil properties. *European Journal of Soil Science*, **46**, 397–414.
- Hengl, T., Heuvelink, G.B.M. & Stein, A. 2004. A generic framework for spatial prediction of soil variables based on regression-kriging. *Geoderma*, **120**, 75–93.
- Heuvelink, G.B.M. & Bierkens, M.F.P. 1992. Combining soil maps with interpolations from point observations to predict quantitative soil properties. *Geoderma*, **55**, 1–15.
- Kerry, R., Rawlins, B.G. & Goovaerts, P. 2010. Area-to-point kriging of organic carbon and soil texture: an efficient use of legacy soil data from polygon maps for regional or national scale digital soil mapping. *Proceedings of 4th Global Workshop on Digital Soil Mapping*, (eds. R. Napoli and R. Francaviglia), pp. 88. Rome, 24–26 May 2010.
- Kyriakidis, P. 2004. A geostatistical framework for area-to-point spatial interpolation. *Geographical Analysis*, **36**, 259–289.
- Liu, Y. & Journel, A.G. 2009. A package for geostatistical integration of coarse and fine scale data. *Computers & Geosciences*, **35**, 527–547.
- Liu, T.L., Juang, K.W. & Lee, D.Y. 2006. Interpolating soil properties using kriging combined with categorical information of soil maps. *Soil Science Society of America Journal*, **70**, 1200–1209.
- McBratney, A.B., Hart, G.A. & McGarry, D. 1991. The use of partitioning to improve the representation of geostatistically mapped soil attributes. *Journal of Soil Science*, **42**, 513–532.
- Pardo-Iguzquiza, E., Atkinson, P.M. & Chica-Olmo, M. 2010. DSCOKRI: a library of computer programs for downscaling cokriging in support of remote sensing applications. *Computers & Geosciences*, **36**, 881–894.
- Rawlins, B.G., Marchant, B.P., Smyth, D., Scheib, C., Lark, R.M. & Jordan, C. 2009. Airborne radiometric survey data and a DTM as covariates for regional scale mapping of soil organic carbon across Northern Ireland. *European Journal of Soil Science*, **60**, 44–54.
- Stein, A., Hoogerwerf, M. & Bouma, J. 1988. Use of map-delineation to improve co-kriging of point data on moisture deficits. *Geoderma*, **43**, 311–325.
- Van Meirvenne, M., Scheldeman, K., Baert, G. & Hofman, G. 1994. Quantification of soil textural fractions of Bas-Zaire using soil map polygons and/or point observations. *Geoderma*, **62**, 69–82.
- Voltz, M. & Webster, R. 1990. A comparison of kriging, cubic splines and classification for predicting soil properties from sample information. *Journal of Soil Science*, **41**, 473–490.
- Wackernagel, H. 1998. *Multivariate Geostatistics*, 2nd edn. Springer, Berlin.
- Webster, R. & Beckett, P.H.T. 1968. Quality and usefulness of soil maps. *Nature*, **219**, 680–682.
- Webster, R., Atteia, O. & Dubois, J.-P. 1994. Coregionalization of trace metals in the soil in the Swiss Jura. *European Journal of Soil Science*, **45**, 205–218.